Tribology Letters (2023) 71:83
https://doi.org/10.1007/s11249-023-01754-z

ORIGINAL PAPER

# Novel Environmentally Superior Tribomaterial with Superlow Friction: 100% Cellulose Nanofiber Molding

Hikaru Okubo[1] · Hiromi Hashiba[2] · Toru Inamochi[2] · Kaisei Sato[3] · Shinya Sasaki[3] · Kazushi Yamada[4] · Ken Nakano[1]

Received: 1 June 2023 / Accepted: 24 June 2023 / Published online: 30 June 2023


## Abstract

In this paper, we report on a novel, environmentally superior tribomaterial with superlow friction of 100% cellulose nanofiber (CNF) molding. Based on our experimental results, the CNF molding exhibited a superlow friction coefficient of approximately 0.01 under lubrication with a fatty acid: glycerin monooleate (GMO) diluted with poly-alfa-olefine. Attenuated total reflection Fourier-transform infrared spectroscopy and high-resolution frequency-modulation atomic force microscopy analyses demonstrated that superlow friction of the CNF molding was realized by GMO-assisted functionalization of the CNF surface, which effectively promoted the formation of a soft absorption film or soft swollen CNF layer. Our findings indicate that the in-situ functionalization of OH-terminated CNF surfaces during the friction process plays a crucial role in achieving superlow friction.

## Graphical Abstract

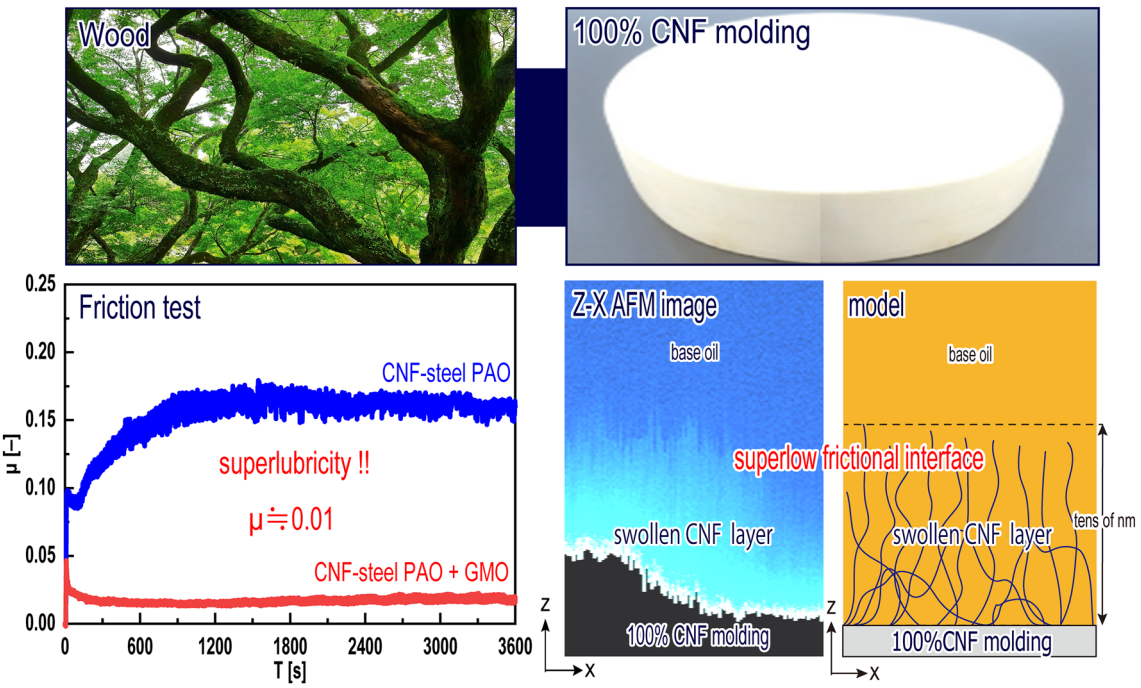


**Keywords** Cellulose nanofibers (CNFs) · Superlow friction · Tribology · Boundary kubrication

Extended author information available on the last page of the article

## 1 Introduction

Against the backdrop of the shift to electric vehicles (EVs), material conversion is a promising approach for developing materials for EV components. Engineering plastics, which have excellent mechanical and thermal properties, have been introduced as substitutes for ferrous-based materials in machine elements owing to their low weight, quietness, and low friction properties [1]. In terms of increasing environmental awareness, a shift to materials for industrial products oriented toward environmental harmony is also being promoted [2–6]. As part of the European Green Deal framework, various regulations have been initiated to reduce the volume of plastic product waste, and it is conceivable that the application of environmentally compatible products could spread to mechanical products such as automobiles in the future [7]. In other words, the future application of engineering plastics for EVs should be regulated. Notably, the introduction of "biological resource-derived (biomass) materials" has previously been considered for tribological machine elements [8]. However, many biomass materials have disadvantageous mechanical properties, thermal stability, dimensional stability, and raw material procurement, resulting in problems when introducing them into machine elements [9]. Against this backdrop, cellulose nanofibers (CNFs) are attracted attention as next-generation biomass industrial materials with 5 times the strength of steel, one-fifth the specific gravity, a low thermal expansion coefficient, and high interface controllability [10–14]. There has been a recent increase in CNF research and industrial applications owing to their excellent properties [15–18]. In particular, CNF-reinforced plastic composite tribomaterials have been developed by many researchers and engineers for tribological applications. The application of CNF-reinforced plastic composites in mechanical sliding materials has previously been reported [19]. However, "plastic-rich" composites, in which CNFs are used as fiber-reinforced materials at low percentage ratios to the base materials, do not make full use of the properties of CNFs because the mechanical and chemical properties are dominated by the bulk plastic materials. Therefore, as part of the development of "CNF-rich" structural materials the authors first considered using high-concentration CNF materials for sliding machine elements and then developed a biomass bulk-material with high strength, light weight, low thermal expansion, and high interface control properties, that is, "100% CNF moldings" (hereafter CNF moldings), obtained by compression molding for CNF dispersions in water [20]. Although CNF moldings have strengths comparable to those of engineering plastics (Fig. S1), there have been no studies on their application under severe operating conditions such as in tribological applications. However, the application of CNF moldings to tribological elements would be a significant breakthrough, accelerating the application of biomass materials to machine elements.

Historically, superlow friction phenomena has received considerable attention in the field if tribology from researchers in academia and industry [21–29]. Previous studies have revealed that solid–liquid interface structures are a key factor in achieving superlow friction at frictional interfaces under boundary lubrication, and the lubrication mechanisms have been reported. De Barros Bouchet et al. [29] suggested that carbon coatings exhibit superlow friction under lubrication with fatty acid oils owing to the formation of a specific solid–liquid interface composed of a fatty acid-derived adsorption layer and a thin graphene oxide layer under boundary lubrication. Long et al. [30] also suggested that a nanometer-thick fluid film, consisting of fatty acids and their degradation products on carbon coatings, prevents direct contact between the solid surfaces, resulting in superlow friction. Watanabe et. al [31] reported on the low-frictional boundary film formation process of a fatty acid diluted with a base lubricant using unique in-situ observation methods. They suggested that the low-friction boundary film was mainly composed of an ordered and adsorbed fatty acid layer that grew gradually and was ordered by frictional motion. Okubo and Sasaki [32] used advanced atomic force microscopy (AFM) to elucidate the formation mechanisms of low-friction boundary films of a fatty acid diluted with a base lubricant. They suggested that the chemical state of frictional substrates is a dominant factor in the growth of a fatty acid-derived adsorption film. Moreover, it is preferable that substrates easily interact with a fatty acid to allow superlow friction phenomena to occur because a fatty acid can form ordered multilayers on such a substrate. Based on the above research, the formation of an ordered fatty acid-derived multilayer or its decompositions anchored to a frictional substrate plays an important role in superlow friction phenomena.

As tribological materials, CNF moldings exhibit outstanding potential in terms of superlow friction owing to the existence of abundant hydroxyl groups on their surfaces that can serve as reactive points to form low-friction fatty acid-derived layers. Many researchers have reported that CNF surfaces can easily be functionalized by fatty acids and other chemicals [33–35]. In this study, we devised an environmentally compatible combination of CNF molding and fatty acids with superlow friction. Tribological tests were carried out using a ball-on-disk tribometer for CNF/steel and steel/steel tribopairs lubricated with polyalphaolefin (PAO) and glycerin monooleate (GMO) diluted with PAO oils. To elucidate the superlow frictional mechanisms of the CNF moldings lubricated with PAO + GMO, attenuated total reflection Fourier transform infrared (ATR-FTIR) spectroscopy, Raman spectroscopy, and high-resolution

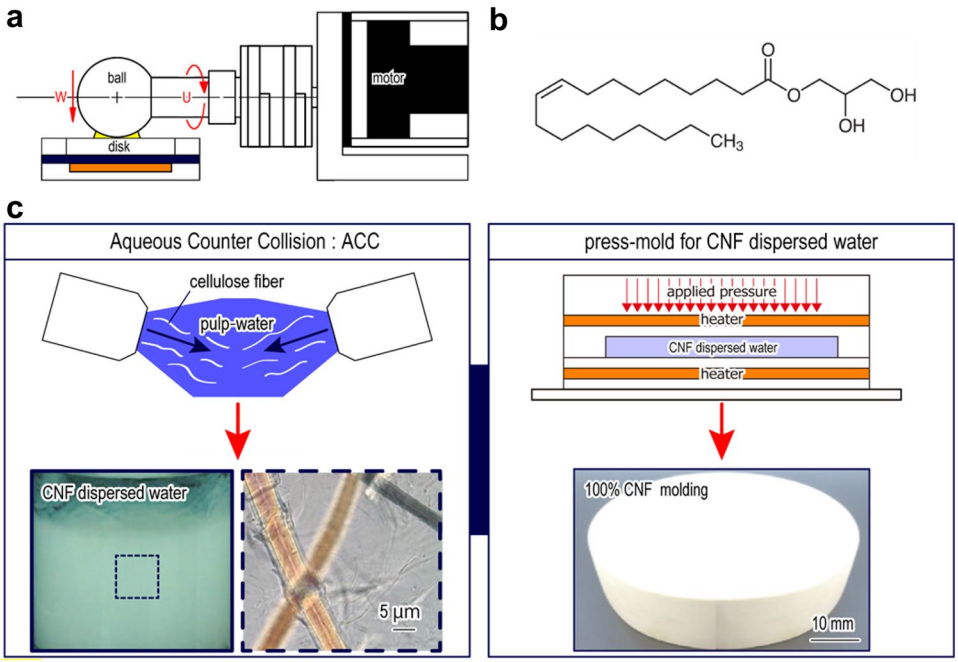


**Fig. 1** **a** Schematic of the tribometer, **b** Chemical structure of glycerin monooleate, **c** schematic of the CNF molding preparation method

frequency-modulation atomic force microscopy (HRFM-AFM) analyses were conducted on the worn surfaces of the CNF moldings.

## 2 Materials and Methods

A ball-on-disk friction tester was used for the friction tests, as shown in Fig. 1a. The experimental conditions were as follows: load = 10 N, Hertz maximum contact pressure ≈ 0.3 GPa (CNF/steel tribopairs), test temperature = 50 °C, relative humidity = 50–70%, sliding speed = 10 mm/s, and sliding time = 60 min. To determine the sliding speed dependency of the friction coefficient, additional friction tests were then performed at sliding speeds of 1.0, 10, 50, 100, and 500 mm/s for each of the 10 sliding cycles. According to the Hamrock–Dowson equations [36, 37], The minimum film thickness was 30 nm under a piezoviscous and elastic regime, and the equivalent surface roughness parameter of the CNF/steel tribopair was 0.1 µm. Hence, the film thickness ratio Λ, calculated as the ratio of the minimum film thickness to the equivalent surface roughness parameter was approximately 0.4. Thus, the friction tests were performed under a mixed or boundary regime.

The lubricant used in this study was a low-viscosity synthetic base oil PAO (kinematic viscosity of 4 cSt at 100 °C). GMO (Fig. 1b) was added to the PAO at 1.0 wt%. AISI52100 bearing steel (HV750, Sa:0.05 µm) was used for the ball (φ19.05 mm) specimen. The AISI52100 bearing steel (HV750, nanoindentation hardness = 10 GPa, $R_a$ = 0.1 µm) and CNF moldings (nanoforest-CMB, JP, density = 1.41 g/cm$^3$, $S_a$ = 0.1 µm, nanoindentation hardness = 0.37 GPa) made from CNF water dispersions prepared by an aqueous counter collision (ACC) method (nanoforest, Chuetsu Pulp & Paper Co, JP) were used as disk specimens (20 × 20 × 5 mm). The preparation procedure for the CNF molding is shown in Fig. 1c.

Laser microscopy (OLS5000, HITACHI, JP), Fourier-transform infrared (FT-IR) spectroscopy (Nicolet iN10, Thermo Fisher Scientific, USA), Raman spectroscopy (LabRAM HR-800, HORIBA, JP), and HRFM-AFM were used for the friction surface analysis. A FT-IR spectroscopic analysis in the attenuated total reflection (ATR) mode was conducted on the worn CNF surfaces with an irradiation time of 30 s, 256 integrations, and the ATR prism of Ge. A Raman analysis was conducted to obtain the crystallinity index of the CNF molding using a laser wavelength of 633 nm to eliminate the influence of fluorescent components on the Raman spectrum. The HRFM-AFM study was conducted on the worn surfaces of the CNF molding immersed in PAO and PAO + GMO to obtain cross-sectional molecular density profiles at the solid–liquid interface [31, 38]. Details of the HRFM-AFM measurements are provided in the Supplementary Information.

## 3 Results

### 3.1 Friction Tests

Friction tests were conducted at the CNF/steel and steel/steel tribopairs lubricated with pure PAO and PAO + GMO.

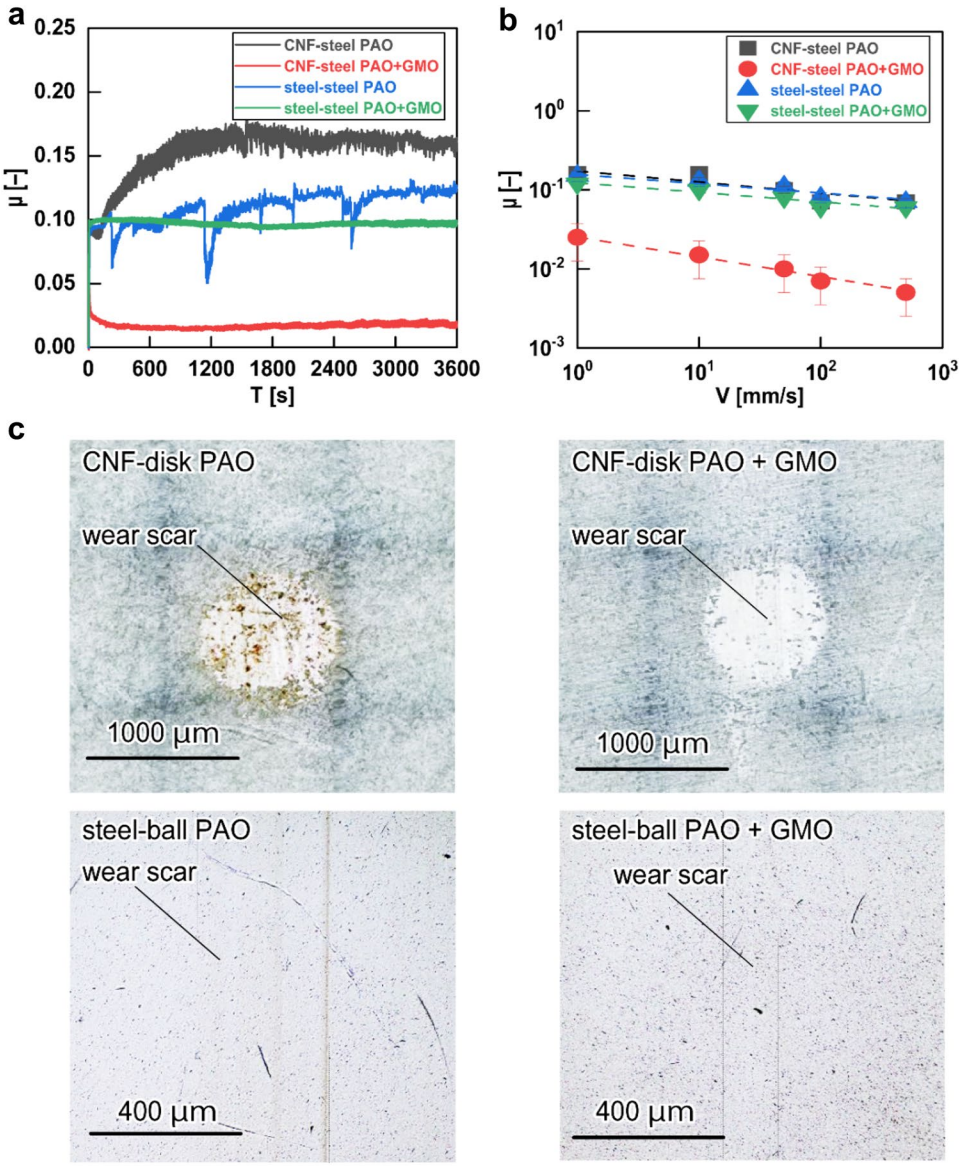


**Fig. 2** **a** Frictional behavior of the CNF/steel and steel/steel tribopairs lubricated with PAO and PAO + GMO. **b** Sliding speed dependance of the friction coefficient for each case. **c** orn surface images of the CNF molding and counter-face steel ball after the friction tests under lubrication with PAO and PAO + GMO

Figure 2a shows the frictional behavior of both tribopairs lubricated with pure PAO and PAO + GMO. Figure 2a shows that the CNF/steel tribopair exhibits a low friction coefficient of 0.01–0.02 under lubrication with PAO + GMO, whereas the other pairs exhibit relatively high friction coefficients of 0.12–0.15, regardless of the lubricants. Figure 2b shows the sliding speed dependence of the friction coefficients for each pair under lubrication with pure PAO and PAO + GMO. The friction coefficient of the CNF/steel tribopair lubricated with PAO + GMO is observed to be one order of magnitude lower than those of the other pairs, regardless of the sliding speeds. Notably, a superlow friction coefficient (< 0.01) is observed at sliding speeds in the range of 50–500 mm/s. Such a remarkably superlow friction phenomenon, which is not observed for the conventional steel/steel tribopair, originates from the CNF molding, triggering the specific chemistry of cellulose surfaces.

The wear scar images of the CNF disks and steel balls for PAO and PAO + GMO (Fig. 2c) show that the appearance of the wear scar on the CNF disks differ for the cases of PAO and PAO + GMO, whereas the appearance of the wear scar on the steel balls was similar in the two cases. For PAO, a light-brown tribofilm formed on the CNF disk, which was confirmed to be composed of iron oxides based on previously reported SEM-EDS and Raman analyses [20]. However, tribofilm formation is not observed on the CNF disk for PAO + GMO. Moreover, contact-mode AFM topographical images of the worn surfaces reveal that the surface roughness of the CNF disk for PAO + GMO is significantly lower than that of the as-molded CNF disk and CNF disk for pure PAO (Fig. S4). Hence, the specific tribochemical interactions that

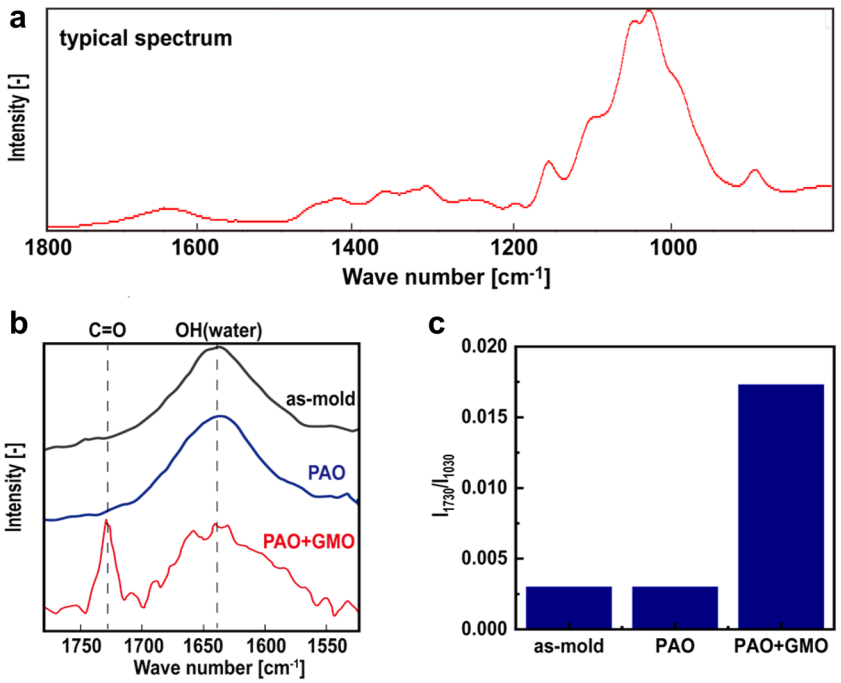


**Fig. 3** **a** Typical ATR-FT-IR spectrum of the CNF molding; **b** ATR FT-IR spectra of the as-molded CNF molding and worn surface of the CNF molding under lubrication with PAO and PAO + GMO; **c** peak intensity ratio of the peaks at 1030 and 1730 $cm^{-1}$

differ from the case of lubrication with PAO occur at the CNF/steel tribopair lubricated with PAO + GMO.

### 3.2 ATR FT-IR Analysis

ATR FT-IR spectroscopic analysis was conducted to reveal the tribo-chemistry that induces superlow friction for the combination of CNF molding and GMO. The ATR FT-IR spectrum of the CNF molding in the wavenumber range of 800–1800 $cm^{-1}$ (Fig. 3a) is a typical spectrum derived from the cellulose structure. The peaks at 897, 1034–1056, 1106, 1156, 1261, 1313, 1366, 1418, and 1650 $cm^{-1}$ were assigned to the group C1 frequency in cellulose I, C–O stretching, ring asymmetric stretching in cellulose I, C–O–C asymmetric stretching in cellulose I, CH bending vibration in cellulose II, $CH_2$ wagging vibration in cellulose II, CH bending vibration in cellulose I and cellulose II, $CH_2$ symmetric bending vibration in cellulose I, and H–O–H bending of water, respectively [39, 40]. Figure 3b shows the spectra of the as-mold CNF surface and worn surfaces of the CNF molding lubricated with PAO and PAO + GMO after the test in the wavenumber range of 1500–1800 $cm^{-1}$. In Fig. 3b, the peak at 1650 $cm^{-1}$ corresponding to the H–O–H bending of water is observed for all cases [40]. However, for the CNF molding lubricated with PAO + GMO, the peak at 1650 $cm^{-1}$ is disturbed; this point is discussed in detail in the Discussion section. In contrast, for the CNF molding lubricated with PAO + GMO, another peak at 1720 $cm^{-1}$ is clearly observed, which is attributed to C = O [41]. Figure 3c shows a comparison of the $I_{1720}/I_{1030}$ peak ratios of the as-molded CNF surface and worn surfaces of the CNF molding lubricated with PAO and PAO + GMO after the test.

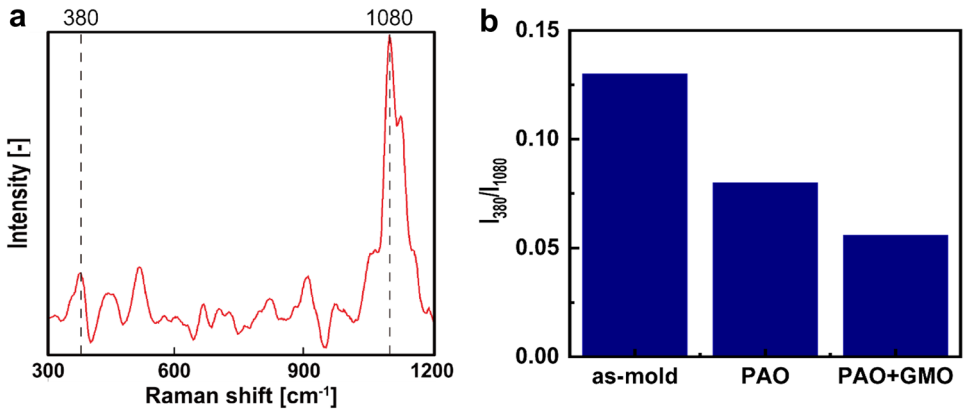


**Fig. 4** **a** Typical Raman spectrum of the CNF molding; **b** crystallinity index: peak intensity ratio of the peaks at 380 and 1080 $cm^{-1}$

The $I_{1720}/I_{1030}$ peak ratio for the CNF molding lubricated with PAO + GMO is significantly higher than those for the other cases, indicating that the GMO with a C = O–O ester structure adsorbed on the CNF molding. In the other words, functionalization reactions occurred on the OH-terminated surfaces of the CNF. In the friction test, the light-brown tribofilm that is iron oxides was observed on the steel disk for PAO whereas the tribofilm did not form on the steel disk for PAO + GMO. Based on the previous study and FT-IR ATR results in this study, the GMO-induced functionalization reactions suppress the formation of iron oxides on the steel disk since the tribochemical reaction for the formation of iron oxides is caused the OH-terminated surfaces of the CNF [20].

### 3.3 Raman Analysis

Raman analysis was conducted on the as-mold and worn CNF moldings lubricated with PAO and PAO + GMO to estimate the friction-induced change in the crystalline structure of the worn CNF molding. Figure 4a shows the typical Raman spectra of the CNF molding, and Fig. 4b shows a comparison of the crystallinity index for the as-mold and worn CNF moldings lubricated with PAO and PAO + GMO [20]. Figure 4a and b show that the crystallinity index $I_{380}/I_{1080}$ has a strong linear correlation with the crystallinity value of the X-ray diffraction calculated from the peaks at 380 and 1080 $cm^{-1}$ assigned to C–C–C, C–C–O, C–O ring deformation, and ring breathing symmetric stretching, respectively, as reported in previous studies [20, 42]. Figure 4b shows that the indexes of both the worn CNF moldings were lower than that of the as-molded CNF molding, indicating that the friction-induced thermal and mechanical effects contributed to the amorphization of the CNF molding. However, the index of the worn CNF molding lubricated with PAO + GMO was lower than that lubricated with PAO, indicating that the friction-induced amorphization of the CNF molding proceeded more than in the other cases despite the friction coefficient of the CNF molding lubricated with PAO + GMO being significantly lower than that of the CNF molding lubricated with PAO. These findings indicate that amorphization proceeds not only owing to friction-induced thermal and mechanical effects but also through the chemical reaction between the CNF molding surface and GMO at the frictional interface.

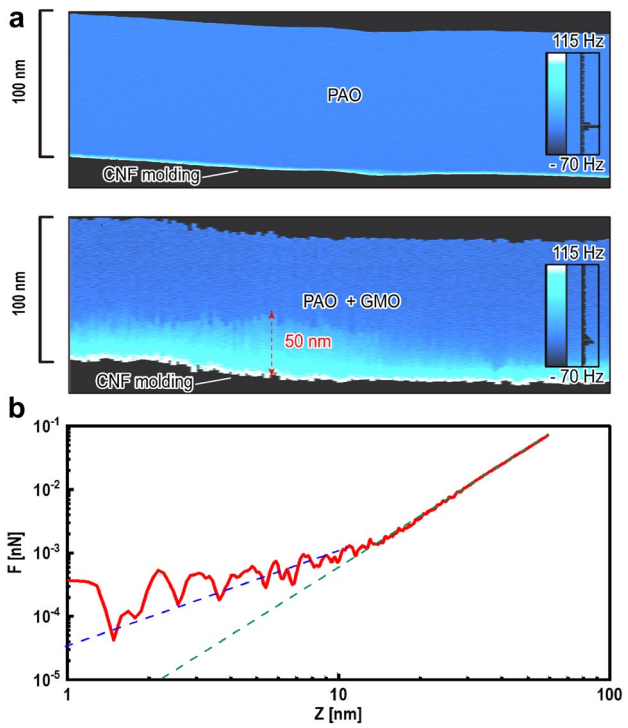


**Fig. 5** h-FM-AFM Z-X frequency shift mapping images of the solid–liquid interface on the CNF moldings for **a** PAO and PAO + GMO; **b** HR-FM-AFM force–displacement curve on the CNF molding for PAO + GMO

### 3.4 HRFM-AFM Analysis

We obtained evidence for CNF surface esterification from the ATR FT-IR spectra, as shown in Fig. 3b and c, indicating the formation of GMO layers adsorbed on the superlow frictional CNF molding surface. To reveal further details of the superlow frictional solid–liquid interface structures of the combination of CNF molding and GMO, a Z–X cross-sectional molecular density visualization analysis was conducted using HRFM-AFM [31]. Figure 5a shows the results of the Z–X cross-sectional molecular density visualization analysis for the worn surfaces of the CNF moldings lubricated with PAO and PAO + GMO. The brighter blue and white regions correspond to regions with a relatively high frequency shift, indicating a relatively high molecular density, whereas the darker blue regions correspond to regions with a relatively low frequency shift, indicating a relatively low molecular density. Figure 5a shows that the relatively high frequency shift region is ~ 1.0 nm for the solid–liquid interface of the CNF molding lubricated with PAO. However, for the solid–liquid interface of the CNF molding lubricated with PAO + GMO, the relatively high frequency shift region is ~ 50 nm. This result suggests the formation of 50-nm-thick layers, corresponding to 20–25 multilayers of GMO, whose molecular size is approximately 2.0–2.5 nm, on the CNF molding. In our previous study [31], we identified the superlow frictional solid–liquid interface of diamond-like carbons lubricated with fatty acids using the HRFM-AFM method, and the thickness of the superlow frictional solid–liquid interface was only ~ 10 nm. A comparison between the present and previous studies reveals that

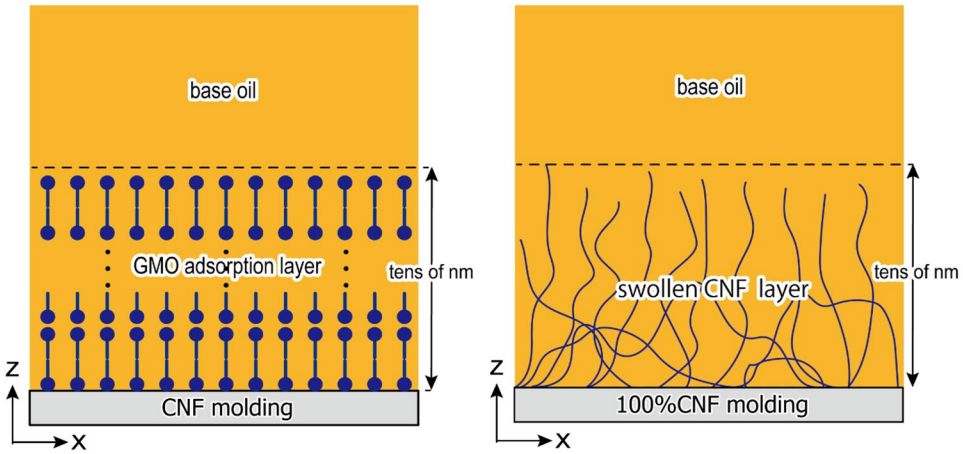


**Fig. 6** **a** Conventional superlow frictional model and **c** novel superlow frictional model for the combined system containing a CNF molding and fatty-acid-containing oils

the superlow frictional adsorbed layers of the combination of CNF molding and GMO are 5 times thicker than the case of the combination of diamond-like carbon and fatty acids. Moreover, such a thick layer is not observed for the steel surface of PAO + GMO, as shown in Fig. S5. Figure 5b shows the force–displacement curve of the solid–liquid interface of the CNF molding lubricated with PAO + GMO. Notably, the frequency shifts of the Z–X mapping images were converted to the applied force of the cantilever using Eq. (8) in the Supplementary Information to describe the force–displacement curve. Based on the Hertzian contact theory fitting for the force–displacement curve in Fig. 5b, the equivalent contact stiffness (E*) of the layer is in the range of 0.01–1.0 kPa (the fitting curve equation: $Y = aX^{3/2}$); indicating that very soft layers formed on the worn CNF moldings lubricated with PAO + GMO. Hence, curious solid–liquid interface structures were formed on CNF moldings when the CNF moldings exhibit superlow friction under lubrication with fatty-acid-containing oils.

## 4 Discussion

We verified the effectiveness of combining CNF moldings and fatty acids for tribological applications. Based on the aforementioned results, the mechanisms underlying the superlow friction of CNF moldings are discussed. Figure 6 schematically shows two hypotheses for the superlow frictional solid–liquid interface of the CNF moldings lubricated with fatty acids. Figure 6a shows a traditional superlow frictional model, which indicates that fatty-acid-derived multilayers play a role in the formation of a protective film that inhibits solid–solid contacts, resulting in low friction. Furthermore, Fig. 6b shows a new superlow frictional model characterized by "swollen GMO-functionalized CNF layers." The ATR FT-IR spectra show that functionalization reactions occur between the CNF surfaces and GMO. Thus, the hydrophobization of the CNF surfaces occurs at the frictional contact point. Cellulose normally forms crystalline domains owing to water-mediated hydrogen bonding [43]. Hence, hydrophobization of the CNF surfaces owing to esterification can result in the degradation of crystalline domains, and CNF can be unwoven both chemically and mechanically during the frictional processes. The degradation of the crystalline domains is evidenced by the Raman analysis results (Fig. 6b), which show that the crystallinity index of the worn CNF molding lubricated with PAO + GMO is significantly lower than that of the as-molded CNF molding and worn surface for PAO. Moreover, thick and soft layers with high molecular densities were obtained, as confirmed by the HRFM-AFM image shown in Fig. 5; therefore, the esterification and unwoven CNFs behave as "brush conformations similar to a cartilage surface" at solid–liquid interfaces, that is, the fatty acid-functionalized unwoven CNFs swell in oils to form soft polymer bush structures at the frictional interfaces. The film thickness of synthesized swollen polymer brushes in solvents is well established as ranging between 10 and 100 nm, and these brushes are soft and exhibit superlow friction [44–48]. The HRFM-AFM results in this study show that the film thickness of the superlow frictional layer is 50 nm, and the layer exhibits a relatively low stiffness. These characteristics are similar to those of polymer brushes [44–48]. In contrast, Nakano and Kono [49] reported that the "vertical lift" of counter-face materials against viscoelastic materials, which is induced by "the damping of the viscoelastic materials," plays a key role in superlow friction performances of soft-mater tribological systems involving polymer brushes and gels since the vertical lift effect via viscoelasticity realizes smooth transition to the fluid film lubrication regime. Hence, if such a solid-interface structure is formed, similar to the hypothesis of the superlow frictional model (Fig. 6b), the fatty-acid-functionalized CNF with a conformation similar to that of the polymer brushes acts as a viscoelastic protective film

and transitions to the fluid film lubrication regime owing to the vertical lift effect caused by the viscoelasticity of the swollen CNF layers, resulting in superlow friction. For all cases, the in-situ functionalization reactions, in conjunction with the OH-terminated surfaces of the CNF, play important roles in achieving superlow friction in the system, although further research is required to determine the superlow frictional model of the CNF molding lubricated with fatty-acid-containing oils. Our results suggest that a combination of 100% CNF moldings and fatty acids is an environmentally superior tribo-system with superlow friction.

## 5 Conclusions

In this study, the superlow friction of the 100% CNF moldings obtained from CNF-dispersed water under lubrication with fatty-acid-containing oils at CNF/steel tribopairs were investigated using several analytical techniques. The conclusions drawn from this study are as follows:

1. The combination of 100% CNF moldings and fatty-acid-containing oils exhibits superlow friction phenomena (μ below 0.01) under a mixed or boundary lubrication regime.
2. Thick and soft layers are formed on 100% CNF moldings owing to friction, and the film thickness of the layer is of the order of tens of nanometers.
3. The superlow friction of 100% CNF moldings can be explained by both the conventional model and new model characterized by a swollen fatty-acid-functionalized CNF layer, which is suggested based on our experimental and analytical results. For all cases, in-situ functionalization reactions acting in conjunction with OH-terminated CNF surfaces play an important role in achieving superlow friction in the system.

**Supplementary Information** The online version contains supplementary material available at https://doi.org/10.1007/s11249-023-01754-z.

**Acknowledgements** The authors are grateful for the support of Mr. Ryota Nakae and Prof. Daisuke Iba at the beginning of this research.

**Author Contributions** The manuscript was written with contributions from all authors. All the authors approved the final version of the manuscript. All authors contributed to the conception and design of this study. Material preparation, data collection, and analyses were performed by HO, TI and HH. The tests and analyses were conducted by HO, KS, and KY. The draft of the manuscript was written by HO and KN. All authors commented on the previous versions of the manuscript. All the authors have read and approved the final version of the manuscript.

**Funding** This work was supported by the JSPS KAKENHI Grant Number JP21K20402, CASIO Science Foundation, MAZDA Science Foundation, and the Transmission Research Association for Mobility Innovation (TRAMI) Foundation.

**Data Availability** The data that support the findings of this study are available from the corresponding author, *Hikaru Okubo*, upon reasonable request.

## Declarations

**Competing Interests** The authors declare no competing interests.



## References

1. Gupta, P., Toksha, B., Patel, B., Rushiya, Y., Das, P., Rahaman, M.: Recent developments and research avenues for polymers in electric vehicles. Chem. Rec. **22**, e202200186 (2022). https://doi.org/10.1002/tcr.20220018
2. Zhou, Y., He, Y., Lin, X., Feng, Y., Liu, M.: Sustainable, high-performance, and biodegradable plastics made from chitin. ACS Appl. Mater. Interfaces. **14**, 46980–46993 (2022). https://doi.org/10.1021/acsami.2c12764
3. Adrah, K., Ananey-Obiri, D., Tahergorabi, R.: Development of bio-based and biodegradable plastics: Novelty, advent, and alternative technology. In: Kharissova, O.V., Torres-Martínez, L.M., Kharisov, B.I. (eds.) Handbook of Nanomaterials and Nanocomposites for Energy and Environmental Applications, pp. 3663–3687. Springer, Cham (2021)
4. Ncube, L.K., Ude, A.U., Ogunmuyiwa, E.N., Zulkifli, R., Beas, I.N.: Environmental impact of food packaging materials: a review of contemporary development from conventional plastics to polylactic acid based materials. Materials (Basel) **13**, 1 (2020)
5. Nandakumar, A., Chuah, J.-A., Sudesh, K.: Bioplastics: A boon or bane? Renew. Sustain. Energy Rev. **147**, 111237 (2021). https://doi.org/10.1016/j.rser.2021.111237
6. Jaiswal, A.K., Hokkanen, A., Kumar, V., Mäkelä, T., Harlin, A., Orelma, H.: Thermoresponsive nanocellulose films as an optical modulation device: proof-of-concept. ACS Appl. Mater. Interfaces **13**, 25346–25356 (2021). https://doi.org/10.1021/acsami.1c03541
7. Kumar, P.: Reduce, reuse, recycle. plastic and packaging waste in the european green deal and circular economy action plan. IASS Discussion Paper (2020)
8. Macqueen, D.J.: Bearings for the biomass boom. IIED Opin. Rep. **17090IIED**, 1–2 (2020)
9. Bustillos, J., Montero, D., Nautiyal, P., Loganathan, A., Boesl, B., Agarwal, A.: Integration of graphene in poly(lactic) acid by 3D printing to develop creep and wear-resistant hierarchical nanocomposites. Polym. Compos. **39**, 3877–3888 (2018). https://doi.org/10.1002/pc.24422
10. Posada, P., Velásquez-Cock, J., Gómez-Hoyos, C., Serpa Guerra, A.M., Lyulin, S.V., Kenny, J.M., Gañán, P., Castro, C., Zuluaga,

R.: Drying and redispersion of plant cellulose nanofibers for industrial applications: a review. Cellulose **27**, 10649–10670 (2020). https://doi.org/10.1007/s10570-020-03348-7
11. Elseify, L.A., Midani, M., Shihata, L.A., El-Mously, H.: Review on cellulosic fibers extracted from date palms (*Phoenix dactylifera* L.) and their applications. Cellulose **26**, 2209–2232 (2019). https://doi.org/10.1007/s10570-019-02259-6
12. Alexandrescu, L., Syverud, K., Gatti, A., Chinga-Carrasco, G.: Cytotoxicity tests of cellulose nanofibril-based structures. Cellulose. **20**, 1765–1775 (2013). https://doi.org/10.1007/s10570-013-9948-9
13. Bondeson, D., Mathew, A., Oksman, K.: Optimization of the isolation of nanocrystals from microcrystalline cellulose by acid hydrolysis. Cellulose. **13**, 171–180 (2006). https://doi.org/10.1007/s10570-006-9061-4
14. Butchosa, N., Zhou, Q.: Water redispersible cellulose nanofibrils adsorbed with carboxymethyl cellulose. Cellulose. **21**, 4349–4358 (2014). https://doi.org/10.1007/s10570-014-0452-7
15. Zhao, Y., Moser, C., Lindström, M.E., Henriksson, G., Li, J.: Cellulose nanofibers from softwood, hardwood, and tunicate: Preparation-structure-film performance interrelation. ACS Appl. Mater. Interfaces. **9**, 13508–13519 (2017). https://doi.org/10.1021/acsami.7b01738
16. El Awad, A., Clarkson, S.M., Moon, C.M., Schueneman, R.J., Youngblood, G.T.: Wet-stacking lamination of multilayer mechanically fibrillated cellulose nanofibril (CNF) sheets with increased mechanical performance for use in high-strength and lightweight structural and packaging applications. ACS Appl. Polym. Mater. **1**, 2525–2534 (2019). https://doi.org/10.1021/acsapm.9b00635
17. El Awad, A., Costakis, S.M., Moon, W.J., Schueneman, R.J., Youngblood, G.T.: Continuous processing of cellulose nanofibril sheets through conventional single-screw extrusion. ACS Appl. Polym. Mater. **2**, 3365–3377 (2020). https://doi.org/10.1021/acsapm.0c00477
18. Rieger, K.A., Cho, H.J., Yeung, H.F., Fan, W., Schiffman, J.D.: Antimicrobial activity of silver ions released from zeolites immobilized on cellulose nanofiber mats. ACS Appl. Mater. Interfaces. **8**, 3032–3040 (2016). https://doi.org/10.1021/acsami.5b10130
19. Sugimoto, M., Yamada, M., Sato, H., Tokumitsu, K.: Reinforcement of polyamide 6/66 with a 9,9′-bis(aryl)fluorene-modified cellulose nanofiber. Polym. J. **51**, 1189–1195 (2019). https://doi.org/10.1038/s41428-019-0238-8
20. Okubo, H., Nakae, R., Daisuke, I., Yamada, K., Yao, S., Nakano, K., Sato, K., Sasaki, S.: Tribological Properties of 100% cellulose nanofiber (CNF) molding under dry and boundary lubricated sliding conditions at CNF/steel contacts. Cellulose. (2023). https://doi.org/10.1007/s10570-023-05309-2
21. Erdemir, A., Eryilmaz, O.L., Fenske, G.: Synthesis of diamond-like carbon films with superlow friction and wear properties. J. Vac. Sci. Technol. A **4**(18), 1987–1992 (2000). https://doi.org/10.1116/1.582459
22. Kano, M.: Super low friction of DLC applied to engine cam follower lubricated with ester-containing oil. Tribol. Int. **39**, 1682–1685 (2006). https://doi.org/10.1016/j.triboint.2006.02.068
23. Kano, M., Yasuda, Y., Okamoto, Y., Mabuchi, Y., Hamada, T., Ueno, T., Ye, J., Konishi, S., Takeshima, S., Martin, J.M., De Barros Bouchet, M.I., Le Mognee, T.: Ultralow friction of DLC in presence of glycerol mono-oleate (GNO). Tribol. Lett. **18**, 245–251 (2005). https://doi.org/10.1007/s11249-004-2749-4
24. Kano, M., Martin, J.M., Yoshida, K., De Barros Bouchet, M.I.: Super-low friction of ta-C coating in presence of oleic acid. Friction. **2**, 156–163 (2014). https://doi.org/10.1007/s40544-014-0047-1
25. Chen, X., Kato, T., Nosaka, M.: Origin of superlubricity in a-C:H:Si films: a relation to film bonding structure and environmental molecular characteristic. ACS Appl. Mater. Interfaces **6**, 13389–13405 (2014). https://doi.org/10.1021/am502416w
26. De Barros Bouchet, M.I., Matta, C., Le-Mogne, T.H., Martin, J.M., Zhang, Q., Goddard, W., Kano, M., Mabuchi, Y., Ye, J.: Superlubricity mechanism of diamond-like carbon with glycerol. coupling of experimental and simulation studies. J. Phys. **89**, 1–14 (2008). https://doi.org/10.1088/1742-6596/89/1/012003
27. Ye, J., Okamoto, Y., Yasuda, Y.: Direct insight into near-frictionless behavior displayed by diamond-like carbon coatings in lubricants. Tribol. Lett. **29**, 53–56 (2008). https://doi.org/10.1007/s11249-007-9281-2
28. Okubo, H., Watanabe, S., Tadokoro, C., Sasaki, S.: Ultralow friction of a tetrahedral amorphous carbon film lubricated with an environmentally friendly ester-based oil. Tribol. Online. **11**, 102–113 (2016). https://doi.org/10.2474/troll.11.102
29. De Barros Bouchet, M.I., Martin, J.M., Avila, J., Kano, M., Yoshida, K., Tsuruda, T., Bai, S., Higuchi, Y., Ozawa, N., Kubo, M., Asensio, M.C.: Diamond-like carbon coating under oleic acid lubrication: evidence for graphene oxide formation in superlow friction. Sci. Rep. **7**, 46394 (2017). https://doi.org/10.1038/srep46394
30. Long, Y., Bouchet, M.B., Lubrecht, T., Onodera, T., Martin, J.M.: Superlubricity of glycerol by self-sustained chemical polishing. Sci. Rep. **9**, 6286 (2019). https://doi.org/10.1038/s41598-019-42730-9
31. Watanabe, S., Tadokoro, C., Miyake, K., Sasaki, S., Nakano, K.: Processes of molecular adsorption and ordering enhanced by mechanical stimuli under high contact pressure. Sci. Rep. **12**, 3870 (2022). https://doi.org/10.1038/s41598-022-07854-5
32. Okubo, H., Sasaki, S.: Frequency-modulation atomic force microscopic observation for ultralow frictional solid-liquidinterface of diamond-like carbon in an environmentally friendly oil. Tribol. Lett. **3** (2019).
33. Peng, S.X., Chang, H., Kumar, S., Moon, R.J., Youngblood, J.P.: A comparative guide to controlled hydrophobization of cellulose nanocrystals via surface esterification. Cellulose. **23**, 1825–1846 (2016). https://doi.org/10.1007/s10570-016-0912-3
34. Sairam, M., Sreedhar, B., Mohan Rao, D.V.M., Palaniappan, S.: Synthesis and thermal degradation kinetics of cellulose esters. Polym. Adv. Technol. **14**, 477–485 (2003). https://doi.org/10.1002/pat.358
35. Sato, A., Kabusaki, D., Okumura, H., Nakatani, T., Nakatsubo, F., Yano, H.: Surface modification of cellulose nanofibers with alkenyl succinic anhydride for high-density polyethylene reinforcement. Compos. A. **1**, 72–79 (2016). https://doi.org/10.1016/j.compositesa.2015.11.009
36. Hamrock, B.J., Dowson, D.: Isothermal elastohydrodynamic lubrication of point contact, part III—fully flooded results. J. Lubr. Tech. **99**, 264–275 (1977). https://doi.org/10.1115/1.3453074
37. Hamrock, B.J., Dowson, D.: Elastohydrodynamic lubrication of elliptical contacts for materials of low elastic modulus I—fully flooded conjunction. J. Lubr. Technol. **100**, 236–245 (1978). https://doi.org/10.1115/1.3453152
38. Hirayama, T., Kawamura, R., Fujino, K., Matsuoka, T., Komiya, H., Onishi, H.: Cross-sectional imaging of boundary lubrication layer formed by fatty acid by means of frequency-modulation atomic force microscopy. Langmuir. **33**, 10492–10500 (2017). https://doi.org/10.1021/acs.langmuir.7b02528
39. Yang, Y.P., Zhang, Y., Lang, Y.X., Yu, M.H.: Structural ATR-IR analysis of cellulose fibers prepared from a NaOH complex aqueous solution. IOP Conf. Ser. Mater. Sci. Eng. **213**, 012039 (2017). https://doi.org/10.1088/1757-899X/213/1/012039
40. Cichosz, S., Masek, A.: IR study on cellulose with the varied moisture contents: insight into the supramolecular structure. Materials (Basel) **13**, 4573 (2020). https://doi.org/10.3390/ma13204573

41. Morris, N.M., Catalano, E.A., Andrews, B.A.K.: FT-IR determination of degree of esterification in polycarboxylic acid cross-link finishing of cotton. Cellulose. **2**, 31–39 (1995). https://doi.org/10.1007/BF00812770
42. Agarwal, U.P., Reiner, R.S., Ralph, S.A.: Cellulose I crystallinity determination using FT-Raman spectroscopy: Univariate and multivariate methods. Cellulose. **17**, 721–733 (2010). https://doi.org/10.1007/s10570-010-9420-z
43. Balasubramaniam, S.L., Patel, A.S., Nayak, B.: Surface modification of cellulose nanofiber film with fatty acids for developing renewable hydrophobic food packaging. Food Packaging Shelf Life. **26**, 100587 (2020). https://doi.org/10.1016/j.fpsl.2020.100587
44. Klein, J., Kumacheva, E., Mahalu, D., Perahia, D., Fetters, L.J.: Reduction of frictional forces between solid surfaces bearing polymer brushes. Nature. **370**, 634–636 (1994). https://doi.org/10.1038/370634a0
45. Heeb, R., Bielecki, R.M., Lee, S., Spencer, N.D.: Room-temperature, aqueous-phase fabrication of poly(methacrylic acid) brushes by UV-LED-induced, controlled radical polymerization with high selectivity for surface-bound species. Macromolecules **42**, 9124–9132 (2009). https://doi.org/10.1021/ma901607w
46. Vlădescu, S.-C., Tadokoro, C., Miyazaki, M., Reddyhoff, T., Nagamine, T., Nakano, K., Sasaki, S., Tsujii, Y.: Exploiting the synergy between concentrated polymer brushes and laser surface texturing to achieve durable superlubricity. ACS Appl. Mater. Interfaces. **14**, 15818–15829 (2022). https://doi.org/10.1021/acsami.2c00725
47. Bueno-Alejo, C.J., Santana Vega, M.S., Chaplin, A.K., Farrow, C., Axer, A., Burley, G.A., Dominguez, C., Kara, H., Paschalis, V., Tubasum, S., Eperon, I.C., Clark, A.W., Hudson, A.J.: Surface passivation with a perfluoroalkane brush improves the precision of single-molecule measurements. ACS Appl. Mater. Interfaces. **14**, 49604–49616 (2022). https://doi.org/10.1021/acsami.2c16647
48. Lupitskyy, R., Roiter, Y., Tsitsilianis, C., Minko, S.: From smart polymer molecules to responsive nanostructured surfaces. Langmuir. **21**, 8591–8593 (2005). https://doi.org/10.1021/la050404a
49. Nakano, K., Kono, M.: Transient and steady sliding friction of elastomers: impact of vertical lift. Front. Mech. Eng. (2020). https://doi.org/10.3389/fmech.2020.00038



## Authors and Affiliations

**Hikaru Okubo[1] · Hiromi Hashiba[2] · Toru Inamochi[2] · Kaisei Sato[3] · Shinya Sasaki[3] · Kazushi Yamada[4] · Ken Nakano[1]**

✉ Hikaru Okubo
okubo-hikaru-xp@ynu.ac.jp

[1] Yokohama National University, Yokohama 240-8501, Japan

[2] Chuetsu Pulp & Paper Co., Ltd., Takaoka 933-8533, Japan

[3] Tokyo University of Science, Katsushika 125-8585, Japan

[4] Kyoto Institute of Technology, Kyoto 606-8585, Japan